Synthesis and Bioconjugation of 2 and 3 nm-Diameter Gold Nanoparticles

ARTICLE *in* BIOCONJUGATE CHEMISTRY · FEBRUARY 2010

Impact Factor: 4.51 · DOI: 10.1021/bc900135d · Source: PubMed

Published in final edited form as:
Bioconjug Chem. 2010 February 17; 21(2): 214–218. doi:10.1021/bc900135d.

Synthesis and Bioconjugation of 2 and 3 nm-diameter Gold Nanoparticles

Christopher J. Ackerson, **Pablo D. Jadzinsky**, **Jonathan Z. Sexton**, **David A. Bushnell**, and **Roger D. Kornberg**
Department of Structural Biology, Stanford School of Medicine, 299 Campus Drive West, Stanford, CA 94305

Abstract

By adjustment of solvent conditions for synthesis, virtually monodisperse 4-mercaptobenzoic acid (*p*-MBA) monolayer-protected gold nanoparticles, 2 and 3 nm in diameter were obtained. Large single crystals of the 2 nm particles could be grown from the reaction mixture. Uniformity was also demonstrated by the formation of two-dimensional arrays and by quantitative high-angle annular dark-field scanning transmission electron microscopy. The 2 and 3 nm particles were spontaneously reactive for conjugation with proteins and DNA, and further reaction could be prevented by repassivation with glutathione. Conjugates with antibody Fc fragment could be used to identify TAP-tagged proteins of interest in electron micrographs, through the binding of a pair of particles to the pair of protein A domains in the TAP tag.

INTRODUCTION

Thiolate-monolayer protected gold nanoparticles (AuNPs) are stable, nanometer-scale metal nanoparticles, passivated by organothiolate monolayers. They have attracted attention for their ease of synthesis, and for their remarkable chemical and electronic properties(1). Synthesis by the method of Brust (2) results in polydisperse products (3), whose size range may be narrowed by purification (4–8), etching (9), annealing (10) or ripening (11). Homogenous thiolate AuNPs coupled to biomolecules, such as DNA or proteins (12,13), hold great promise for electron microscopy (14), nanoscale construction (15), enzyme enhancement (16), and other applications.

We previously reported the formation of a linker-free bond between a thiolate AuNP and a protein (17). The method entailed a chemical oxidation step to activate the AuNP (18), followed by protein conjugation, and reduction to quench AuNP reactivity. As conjugation was incomplete, gel filtration was performed to remove unreacted protein and AuNP. The limitations of this work were a residual size heterogeneity of the purified AuNPs, the requirement for multiple steps of activation and deactivation, and incomplete conjugation.

We have now overcome these limitations, through the direct synthesis of essentially homogeneous thiolate AuNPs, a high intrinsic reactivity of the AuNPs, and efficient protein conjugation. The choice of thiolate and the conditions for AuNP synthesis were important

kornberg@stanford.edu .
Present addresses: C.J. Ackerson, Department of Chemistry, Colorado State University, Fort Collins, CO. Ackerson@stanfordalumni.org; P.D. Jadzinsky, Department of Neurobiology jadz@stanford.edu, Stanford University; J.Z. Sexton, Biomanufacturing Research Institute and Technology Enterprise, North Carolina Central University, Durham, NC.

Supporting Information Available: Full details of the synthesis, supporting figures referenced in the text, and optical electronic spectra are available included in the supporting information. This information is available free of charge via the Internet at http://pubs.acs.org/.

for these advances. The implications extend beyond the particular examples and applications described to the formation and structure of thiolate AuNPs in general.

EXPERIMENTAL SECTION / MATERIALS AND METHODS

Nanoparticle synthesis

Screening of reaction conditions was performed in 96 well plates with 1 ml total volume per well. Following a reaction time of about 16 hours, product was precipitated by addition of 2 mL methanol, product was collected by centrifugation, the supernatant was removed, and product was re-dissolved in 50% aqueous glycerol. Product was analyzed by 15T/5C Tris-borate EDTA buffered polyacrylamide gel electrophoresis (TBE-PAGE), at no more than 150V, until a satisfactory separation was observed in the gel. Reaction conditions explored in this manner included pH (2–13), *p*-MBA:Au(III) ratio (0.5:1 – 10:1), $NaBH_4$:Au(III) ratio (0.5:1 – 10:1), and concentration of aqueous methanol (5% to 95%). Synthesis of 3 nm AuNPs was identical to that of 2 nm AuNPs except that it was accomplished in 87% aqueous methanol. Further details of nanoparticle synthesis may be found in Section S1 of the Supporting Information.

Protein conjugation

For analytical purposes, a mixture containing 0.8 μg of candidate protein, 300 μM Tris-carboxy ethyl phosphine (TCEP), and 200 μM Au_{144} AuNP was incubated in a total volume of 15 μl at 37°C for 1 h. Control reactions contained water instead of Au_{144} AuNP. The reaction mixture was combined with an equal volume of 50% glycerol and fractionated by sodium dodecyl sulfate (SDS) PAGE (12%/3.3C) for 1 h at 150 V.

Preparative gel electrophoresis

In order to drive the reaction to completion, a large excess of AuNP:scFv was used. Excess AuNP was removed by native gel electrophoresis. Up to 5 ml of sample may be loaded and separated in a 5T/5C TBE buffered acrylamide gel, in a Bio-Rad Mini-Protean III gel electrophoresis apparatus, with 1.5 mm plate spacing and a single well preparative comb, run at 80 V constant voltage. The bands are visible in the gel without enhancement by stain, due to the visible absorption of the AuNP. The bands may be excised with a razor blade, crushed by passing through a syringe, and eluted into a desired buffer.

Repassivation

In a typical repassivation experiment, a series of 15 two-fold dilutions of glutathione (GSH), varying from 650 mM to 20 μM, was prepared. Equal volumes (3 μl) of glutathione solution and gold/protein (500 μg/ml) or gold/DNA conjugate were mixed and incubated for 1 h at 37°C, followed by analysis by 12T/3.3C or 10T/5C PAGE for gold/protein and gold/DNA conjugates, respectively.

Electron Microscopy

Particles shown in figures 2, S1, S2, and S3 were drop cast on 400 mesh glow discharged carbon-coated copper electron microscope (EM) grids (EM Sciences), and examined in an FEI CM12 EM, operated at 100kV accelerating voltage.

Cryo-EM

Samples (3μL,approximately 0.2mg protein/mL) were deposited on copper quantifoil grids (R2/4 spacing), blotted, and plunge-frozen in liquid ethane with an automated vitrification apparatus. Samples were imaged in a liquid-nitrogen cooled FEI Tecnai G2 Polara with an acceleration voltage of 300kV. Images were recorded on a 2k × 2k Peltier-cooled CCD

camera (Tietz TemCam-F224HD). Images were recorded at −2μ underfocus to enhance the visibility of the nanoparticles. Contrast transfer function correction was not performed, so protein density was not visible at this underfocus.

RESULTS

Nanoparticle Synthesis

Brust synthesis is accomplished in a two-step reaction, by mixing a 3-fold molar excess of organic thiol and a trivalent gold salt, with a phase transfer catalyst if necessary, to produce a gold-thiol polymer, which is then reduced with borohydride. The effects of varying the thiol:gold ratio and borohydride^{-} concentration have been widely reported. When a water-soluble product is synthesized, the reaction is typically performed in aqueous methanol. We undertook a systematic exploration of conditions for synthesis of *p*-MBA -protected gold AuNPs (19,20), varying the pH, reactant concentration, reduction time, and aqueous methanol concentration.

Reaction products were analyzed by polyacrylamide gel electrophoresis (PAGE) (7), and those with narrow size distributions were further analyzed by EM. Optimal yields of AuNPs were obtained with a pH of 13, a *p*-MBA: Au(III) mole ratio of 3.4:1, and an Au(III) concentration of 10 μM. Longer reduction (16–18 h) with less borohydride produced more uniform product than shorter reaction with more borohydride.

The percentage of methanol in the reaction affected both the size and uniformity of the product. Reactions performed in 27% and 87% aqueous methanol gave nearly uniform AuNPs, as shown by sharp bands in PAGE (Figure 1) and the formation of two-dimensional ordered arrays on EM grids (Figure 2, Supporting Information Figure S2). Approximate diameters of 2.0 and 3.0 nm were measured for the AuNPs. At other methanol concentrations, heterogeneous particles were obtained (Supporting Information, Figure S3).

The exceptional uniformity of the 2 nm AuNPs prompted an attempt at crystallization. In the presence of various salts, including sodium chloride and sodium borate (at least 0.15 M), and ammonium acetate (at least 0.2 M), single crystals were obtained. The largest crystals, approximately 300 μ in longest dimension, were produced by slow evaporation from sodium chloride solution, and gave diffraction to 5.5 Å resolution (Supporting Information, Figure S4.) A similar synthesis, differing only in the pH prior to borohydride reduction, led to crystals of a 1.5 nm particle diffracting to 1.1Å resolution (21).

The 2 nm AuNPs were further characterized by quantitative high-angle annular dark-field scanning transmission EM (HAADF-STM). A value of 144±22 atoms for the gold core was obtained (Supporting Information, Figure S5.) For comparison, HAADF-STM gives a value of 13.6±3.4 atoms for the gold core of an Au_{13} particle(22). The 15% standard deviation in the measurement of the 2 nm particles compares favorably with the 25% standard deviation in the measurement of the Au_{13} particle. Much of the measurement error may attributed to unevenness in the carbon support film. The ^{1}H NMR spectrum of the 2 nm AuNP displayed a broad band centered on the positions of the peaks from *p*-MBA, confirming the surface immobilization of the *p*-MBA and the absence of any chemical alteration by exposure to high pH or borohydride (Supporting Information, Figure S6). The UV/Visible spectrum of the 2 nm AuNPs (Supporting Information, Figure S11) included peaks at ~300 and ~510nm, and was similar to the spectrum of the well studied “29 kDa compound,”[I] (23, 24, 25, 26). This compound has recently been analyzed by high resolution mass spectroscopy and reported to have a core of Au_{144}. (25, 26)

Reaction of *p*-MBA AuNPs with cysteine-mutant proteins and thiolated DNA

In our previous work, glutathione AuNPs were activated by oxidation with permanganate for conjugation with the "NC10" scFv antibody fragment (17). Single cysteine residues were introduced at or near the C-terminus of NC10 for the purpose. Substitution mutants S112C and A113C contained cysteines in place of the last two structured residues of NC10 revealed by X-ray diffraction. C-terminal extension mutants 114C – 118C contained cysteines one to five positions beyond the last structured residue. In addition, in mutants L15C, Q80C, G15C, and P14C, cysteines were substituted for surface residues elsewhere in the "framework" region of NC10. Glutathione AuNP conjugates were only obtained with C-terminal extension mutants 116C – 118C, showing a requirement for exposure of the cysteine residue for reactivity (17). In contrast, the 2 nm *p*-MBA AuNP reacted with all NC10 mutants, resulting in a characteristic gel shift upon SDS-PAGE (Figure 3). Conjugate formation was essentially quantitative, except in the case of S112C, L15C, Q80C, and G15C mutants, whose reactivity was slightly diminished. A surface cysteine mutant of catalase, K560C, showed no reactivity at all (Supporting Information, Figure S7). The 2 nm *p*-MBA AuNP reacted rapidly and quantitatively with synthetic oligonucleotides bearing terminal thiol groups (27) (Supporting Information, Figure S8.)

Reaction of *p*-MBA AuNPs with native cysteine residues in proteins, and detection by EM

Reaction of *p*-MBA AuNPs was tested with two proteins bearing native cysteine residues, muscle actin and antibody Fc fragment. The 2 nm *p*-MBA AuNP formed conjugates with three of seven cysteines in muscle actin, as shown by SDS-PAGE (Supporting Information, Figure S9). Antibody Fc fragment contains two polypeptide chains with a disulfide bond between them. Following reduction of the disufide bond with TCEP, reaction with both 2 nm and 3 nm *p*-MBA AuNPs was observed. Detection in this case took advantage of the strong binding of Fc fragments to protein A, in particular to the two protein A domains in the widely used Tandem Affinity Purification (TAP) tag (28). EM of AuNP – Fc bound to TAP-tagged protein showed pairs of closely apposed gold particles. These pairs of particles were clearly attributable to conjugates, and distinguishable from unreacted AuNP – Fc, scattered across the micrographs, on the basis of their characteristic spacing (Figure 4).

Quenching *p*-MBA AuNP reactivity

In order to quench the reactivity of *p*-MBA AuNP – protein conjugates towards further protein sulfhydryls, we took advantage of the unreactivity of glutathione AuNPs noted previously. Treatment of the 2 nm *p*-MBA AuNP with 1 mM glutathione for one h at room temperature proved effective for the purpose. We presume the product was repassivated (most or all *p*-MBA replaced by glutathione) because the AuNP remained intact (Supporting Information, Figure S10), while reactivity was lost. Following conjugation and repassivation, NC10 scFv retained affinity for its antigen, the tetrameric N9 neuraminidase, as shown by mixing with neuraminidase and cryo-EM. Characteristic sets of four gold particles were observed (Figure 5). The DNA in repassivated AuNP conjugates also remained capable of interaction, as shown by hybridization with complementary strand and gel electrophoresis.

[I]There are at least 4 previous reports of UV/VIS spectra for the "29 kDa" or Au_{144} compound, found in references 23, 24, 25, and 26. Each of these spectra differs in `fine detail' but a hallmark of this compound is a very small surface-plasmon resonance-like inflection or peak at 510nm or 2.4eV. Differences between the three spectra and the spectrum accompanying our report may be accounted for by differences in the ligand comprising the monolayer and by differences in instrument sensitivity.

DISCUSSION

The notable results of this work include the following: the effect of solvent on the products of *p*-MBA AuNP synthesis; the formation of virtually monodisperse 2 nm and 3 nm particles; the growth of large single crystals of the 2 nm particle amenable to X-ray diffraction analysis; the spontaneous reactivity of *p*-MBA particles towards protein and DNA sulfhydryls; the quenching of reactivity by repassivation with glutathione; and a method for distinguishing particles bound to proteins of interest from free particles by EM.

On the basis of transmission EM, HAADF-STEM, and UV-VIS spectroscopy, we identify the 2 nm particle as having an Au_{144} core, consistent with other recent assignments for an AuNP often referred to as a “29 kDa” compound. An important contribution of our work is the direct synthesis, with no requirement for purification, annealing, ripening, or etching to obtain an essentially monodisperse product, as judged from the formation of single crystals, from an exceptionally narrow band in PAGE, from HAADF – STEM, and from TEM.

The 2 nm particles were insoluble at methanol concentrations above 27% (Figure 1, right panel). The uniformity of the particles may therefore be due, in part, from growth in solution to a critical size, at which precipitation occurs. The 3 nm particles appeared less uniform than the 2 nm particles and did not precipitate at the methanol concentration used. Their size distribution may be narrowed by a reduced reaction rate under the high pH conditions used. Others have suggested that reducing the rate of reduction may allow the creation of more uniform particles (29). We have observed that the color change indicative of particle formation requires hours for reactions performed at high pH, as opposed to seconds for reactions at low pH.

Metal nanoparticles are believed to be stabilized by electronic shell filling for smaller particles and geometric shell filling for larger particles. The concept of shell filling leads naturally to the idea of `magic number' series. In the case of gold AuNPs, nominal inorganic masses of 5, 8, 15, 20, 29, 45, and 93 kDa have been derived (6,30,31). Recent X-ray structure determination of the 5 kDa (Au_{25}) (32) and 20 kDa (Au_{102}) (21) compounds led to the conclusion that even particles as large as Au_{102} are stabilized as electronic shell filling (33).

The structure and exact formulation of the 29 kDa compound — which we identify here as an Au_{144} 2 nm particle – remains a matter of conjecture. For 144 gold atoms, closure of a 90e- or 92e- electronic shell would require 52 or 54 ligands (on the assumption that each gold atom donates one electron and each *p*-MBA group withdraws one electron from the electronic shell) (33). This argument is called into question, however, by recent mass spectroscopy, which led to a formulation of the 29 kDa compound as $Au_{144}(SR)_{59}$ (24) and a DFT calculation which argued for an assignment of $Au_{144}(SR)_{60}$ (34).

Our previous work (15) established a method for the formation of rigid, specific and discrete gold nanoparticle/protein conjugates. The method yields a direct bond between gold atoms of the gold nanoparticle core and the sulfhydryl moiety of a cysteine residue, whereas the commercial product, Nanogold (Nanoprobes, Yaphank, NY), relies on a flexible organic linker and a maleimide group to accomplish binding to cysteine residues. The elimination of the linker facilitates applications requiring rigid immobilization of AuNPs on proteins. Conjugates formed by electrostatic interaction with `traditional' colloidal gold may also be rigid, but will not necessarily have a precise number of AuNPs bound at the same location on every protein.

In contrast to our previous work with glutathione AuNPs, the formation of protein and DNA conjugates with *p*-MBA AuNPs was more facile and more promiscuous. Whereas the

reaction of activated glutathione AuNPs with scFvs bearing reduced, exposed cysteine residues never surpassed 50%, the *p*-MBA AuNPs reacted quantitatively with exposed cysteine residues. Moreover, while glutathione AuNPs showed only slight reactivity towards the 116C extension mutant of the NC10 scFv, and no reactivity towards the shorter 115C, 114C, A113C, and S112C extension mutants, *p*-MBA AuNPs reacts almost quantitatively with mutants 114C and longer.

The high reactivity of *p*-MBA AuNPs may in some cases capture nonnative conformations of the scFv or other protein target. While most conjugates formed with the NC10 scFv retained affinity for the N9 neuraminidase antigen, conjugates with the Q80C framework mutant of NC10 showed diminished affinity. The failure of conjugate formation with the K560C mutant of catalase is important in this regard. The cysteine residue in the K560C mutant is located in a depression on the protein surface, rendering it inaccessible to an AuNP of the diameter used (Supporting Information, Figure S7). The AuNP evidently did not induce protein denaturation sufficient for reactivity.

Supplementary Material

Refer to Web version on PubMed Central for supplementary material.

Acknowledgments

We thank Laurent Menard and Ralph Nuzzo for HAADF-STM analysis, Peter Loewen for catalase and catalase mutants, and Corey Liu and the SMRL for NMR. We also thank Pamela Bjorkman and Grant Jensen for their interest in large gold AuNPs, which stimulated our work. Portions of this research were carried out at the Stanford Synchrotron Radiation Laboratory, a national user facility operated by Stanford University on behalf of the U.S. Department of Energy, Office of Basic Energy Sciences. The SSRL Structural Molecular Biology Program is supported by the Department of Energy, Office of Biological and Environmental Research, and by the National Institutes of Health, National Center for Research Resources, Biomedical Technology Program, and the National Institute of General Medical Sciences. This research was supported by NSF grant CHE-0617050 and NIH grant AI21144.

References

(1). Daniel M, Astruc D. Gold nanoparticles: assembly, supramolecular chemistry, quantum-size-related properties, and applications toward biology, catalysis, and nanotechnology. Chem. rev. 2004; 104:293–346. [PubMed: 14719978]

(2). Brust M, Fink J, Bethell D, Schiffrin DJ, Kiely C. Synthesis and reactions of functionalized gold nanoparticles. J. Chem. Soc., Chem. Comm. 1995:1655–6.

(3). Alvarez MM, Khoury JT, Schaaff TG, Shafigullin MN, Vezmar I, Whetten RL. Critical sizes in the growth of Au clusters. Chem. Phys. Lett. 1997; 266:91–98.

(4). Peterson RR, Cliffel DE. Continuous free-flow electrophoresis of water-soluble monolayer-protected clusters. Anal. Chem. 2005; 77:4348–53. [PubMed: 16013845]

(5). Schaaff TG, Knight G, Shafigullin MN, Borkman RF, Whetten RL. Isolation and Selected Properties of a 10.4 kDa Gold:Glutathione Cluster Compound. J. Phys. Chem. B. 1998; 102:10643–10646.

(6). Whetten RL, Khoury JT, Alvarez MM, Murthy S, Vezmar I, Wang ZL, Stephens PW, Cleveland CL, Luedtke WD, Landman U. Nanocrystal gold molecules. Adv. Mater. 1996; 8:428–33.

(7). Schaaff TG, Whetten RL. Controlled Etching of Au:SR Cluster Compounds. J. Phys. Chem. B. 1999; 103:9394–9396.

(8). Whetten RL, Khoury JT, Alvarez MM, Murthy S, Vezmar I, Wang ZL, Stephens PW, Cleveland CL, Luedtke WD, Landman U. Nanocrystal gold molecules. Advanced Materials (Weinheim, Germany). 1996; 8:428–33.

(9). Schaaff TG, Whetten RL. Isolation and Selected Properties of a 10.4 kDa Gold:Glutathione Cluster Compound. J. of Phys. Chem. B. 1999; 102:10643–6.

(10). Hicks JF, Miles DT, Murray RW. Quantized double-layer charging of highly monodisperse metal nanoparticles. J. Am. Chem. Soc. 2002; 124:13322–8. [PubMed: 12405861]

(11). Prasad BLV, Stoeva SI, Sorensen CM, Klabunde KJ. Digestive Ripening of Thiolated Gold Nanoparticles: The Effect of Alkyl Chain Length. Langmuir. 2002; 18:7515–7520.

(12). Aubin-Tam ME, Hwang W, Hamad-Schifferli K. Site-directed nanoparticle labeling of cytochrome c. Proc. Natl. Acad. Sci. U S A. 2009; 106:4095–100. [PubMed: 19251670]

(13). Aubin-Tam ME, Hamad-Schifferli K. Gold nanoparticlecytochrome C complexes: the effect of nanoparticle ligand charge on protein structure. Langmuir. 2005; 21:12080–4. [PubMed: 16342975]

(14). Jensen GJ, Kornberg RD. Single-particle selection and alignment with heavy atom cluster-antibody conjugates. Proc. Natl. Acad. Sci. U S A. 1998; 95:9262–9267. [PubMed: 9689068]

(15). Zanchet D, Micheel CM, Parak WJ, Gerion D, Alivisatos AP. Electrophoretic isolation of discrete Au nanocrystal/DNA conjugates. Nano Lett. 2001; 1:32–35.

(16). Xiao Y, Patolsky F, Katz E, Hainfeld JF, Willner I. “Plugging into Enzymes”: nanowiring of redox enzymes by a gold nanoparticle. Science. 2003; 299:1877–81. [PubMed: 12649477]

(17). Ackerson CJ, Jadzinsky PD, Jensen GJ, Kornberg RD. Rigid, specific, and discrete gold nanoparticle/antibody conjugates. J. Am. Chem. Soc. 2006; 128:2635–40. [PubMed: 16492049]

(18). Song Y, Murray RW. Dynamics and Extent of Ligand Exchange Depend on Electronic Charge of Metal Nanoparticles. J. Am. Chem. Soc. 2002; 124:7096–7102. [PubMed: 12059234]

(19). Johnson SR, Evans SD, Brydson R. Influence of a Terminal Functionality on the Physical Properties of Surfactant-Stabilized Gold Nanoparticles. Langmuir. 1998; 14:6639–6647.

(20). Ackerson CJ, Jadzinsky PD, Kornberg RD. Thiolate ligands for synthesis of water-soluble gold clusters. J. Am. Chem. Soc. 2005; 127:6550–1. [PubMed: 15869273]

(21). Jadzinsky PD, Calero G, Ackerson CJ, Bushnell DA, Kornberg RD. Structure of a thiol monolayer-protected gold nanoparticle at 1.1 A resolution. Science. 2007; 318:430–3. [PubMed: 17947577]

(22). Menard LD, Gao SP, Xu H, Twesten RD, Harper AS, Song Y, Wang G, Douglas AD, Yang JC, Frenkel AI, Nuzzo RG, Murray RW. Sub-nanometer Au monolayer-protected clusters exhibiting molecule-like electronic behavior: Quantitative high-angle annular dark-field scanning transmission electron microscopy and electrochemical characterization of clusters with precise atomic stoichiometry. J. Phys. Chem. B. 2006; 110:12874–83. [PubMed: 16805585]

(23). Wyrwas RB, Alvarez MM, Khoury JT, Price RC, Schaaff TG, Whetten RL. The colours of nanometric gold - Optical response functions of selected gold-cluster thiolates. Eur. Phys. J. D. 2007; 43:91–5.

(24). Schaaff TG, Shafigullin M, Khoury J, Vezmar I, Whetten RL. Properties of a Ubiquitous 29 kDa Au:SR Cluster Compound. J. Phys. Chem. B. 2001; 105:8785–8796.

(25). Huifeng, Q.; Jin, R. Controlling Nanoparticles with Atomic Precision: The Case of $Au_{144}(SCH_2CH_2Ph)_{60}$. 2009. Epub before print, DOI: 10.1021/nl902300y

(26). Chaki NK, Negishi Y, Tsunoyama H, Shichibu Y, Tsukuda T. Ubiquitous 8 and 29 kDa gold:alkanethiolate cluster compounds: mass-spectrometric determination of molecular formulas and structural implications. J. Am. Chem. Soc. 2008; 130:8608–10. [PubMed: 18547044]

(27). Ackerson CJ, Sykes MT, Kornberg RD. Defined DNA/nanoparticle conjugates. Proc. Natl. Acad. Sci. U S A. 2005; 102:13383–5. [PubMed: 16155122]

(28). Rigaut G, Shevchenko A, Rutz B, Wilm M, Mann M, Seraphin B. A generic protein purification method for protein complex characterization and proteome exploration. Nat. Biotechnol. 1999; 17:1030–2. [PubMed: 10504710]

(29). Zheng N, Fan J, Stucky GD. One-step one-phase synthesis of monodisperse noble-metallic nanoparticles and their colloidal crystals. J. Am. Chem. Soc. 2006; 128:6550–1. [PubMed: 16704242]

(30). Cleveland CL, Landman U, Schaaff TG, Shafigullin MN, Stephens PW, Whetten RL. Structural evolution of smaller gold nanocrystals: The truncated decahedral motif. Phys. Rev. Lett. 1997; 79:1873–1876.

(31). Cleveland CL, Landman U, Shafigullin MN, Stephens PW, Whetten RL. Structural evolution of larger gold clusters. Z. Phys. D. 1997; 40:503–508.

(32). Heaven MW, Dass A, White PS, Holt KM, Murray RW. Crystal Structure of the Gold Nanoparticle [N(C(8)H(17))(4)][Au(25)(SCH(2)CH(2)Ph)(18)]. J. Am. Chem. Soc. 2008; 130:5940–6. [PubMed: 18393500]

(33). Walter M, Akola J, Lopez-Acevedo O, Jadzinsky PD, Calero G, Ackerson CJ, Whetten RL, Gronbeck H, Hakkinen H. A unified view of ligand-protected gold clusters as superatom complexes. Proc. Natl. Acad. Sci. U S A. 2008; 105:9157–62. [PubMed: 18599443]

(34). Lopez-Acevedo O, Akola J, Whetten RL, Gronbeck H, Hakkinen H. Structure and Bonding in the Ubiquitous Icosahedral Metallic Gold Cluster Au-144(SR)(60). J. Phys. Chem. C. 2009; 113:5035–8.

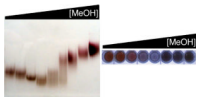

Figure 1.
PAGE (15T/5C) revealing changes in product size and dispersity as a function of methanol concentration (from left to right, 7, 17, 27, 37, 47, 57, 67, 77, and 87% methanol) (left panel). The deep red color of the leftmost reactions indicates soluble product and the black color of the rightmost reactions indicates insoluble product. A reaction performed in 27% methanol, which produced 2 nm particles, is in the third well from the left.

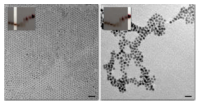

Figure 2.
Transmission EM images of MPCs produced in 27% methanol (left panel) and 87% methanol (right panel). Scale bar represents 10 nm.

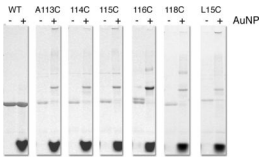

Figure 3.

scFv reactivity. The leftmost gel shows the wild-type (WT) NC10 scFv in the presence (+) and absence (−) of gold. To the right is the A113C “nested mutant” in which a gel-shifted band appears in the presence of the 2nm AuNP. The shifted band was observed in the presence of AuNP for all mutants of the NC10 scFv tested

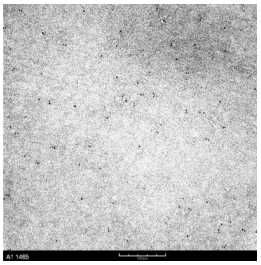

Figure 4.
TAP-tagged RNA polymerase was incubated with Fc/2 nm particle conjugates and drop cast onto a carbon coated EM grid.

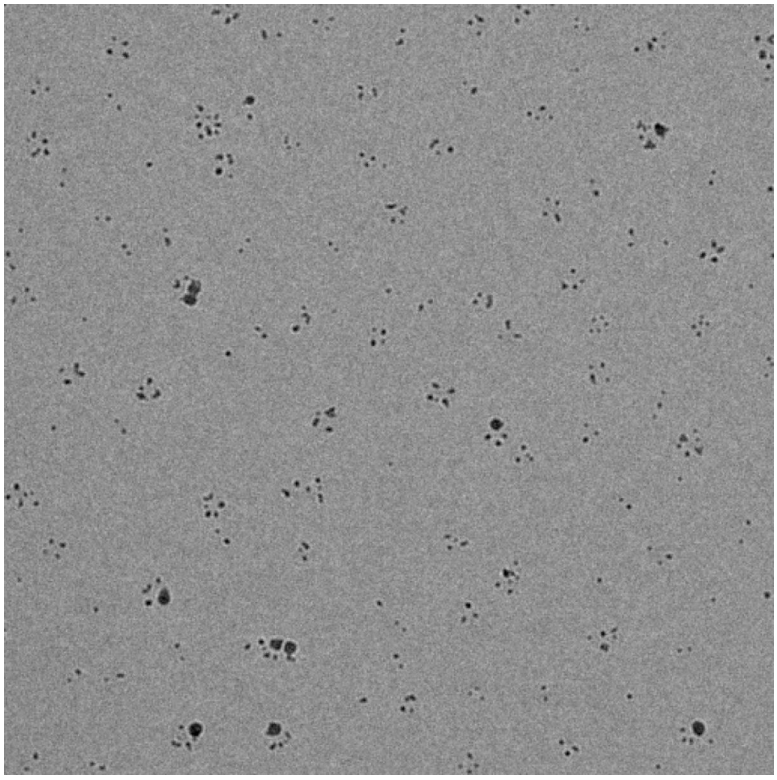

Figure 5.
Cryo-EM of NC10/2 nm AuNP mixed with N9 neuraminidase. The tetrameric structure of N9 neuraminidase results in binding of four scFv fragments. The larger particles observed are 10 nm AuNP, included as markers in this cryo-EM preparation.